Journal of Power Sources 225 (2013) 207–214

Contents lists available at SciVerse ScienceDirect

Journal of Power Sources

journal homepage: www.elsevier.com/locate/jpowsour

Short communication

Elastic softening of alloy negative electrodes for Na-ion batteries

Majid Mortazavi [a], Junkai Deng [a], Vivek B. Shenoy [b,**], Nikhil V. Medhekar [a,*]

[a] Department of Materials Engineering, Monash University, Clayton, Victoria 3800, Australia
[b] Department of Materials Science and Engineering, University of Pennsylvania, Philadelphia, PA 19104, USA

HIGHLIGHTS

- We obtain the intrinsic elastic properties of alloy anodes for Na-ion batteries.
- We have investigated sodiation of Na–M (M = Sn, Pb, Si, Ge) alloys for anodes.
- Sodiation of these alloys leads up to 75% deterioration of their elastic moduli.
- Elastic softening arises due to a transition to weak ionic interatomic bonding.
- These results provide the first step in developing models for failure in Na anodes.

ARTICLE INFO

Article history:
Received 26 July 2012
Received in revised form
11 September 2012
Accepted 12 October 2012
Available online 23 October 2012

Keywords:
Na-ion batteries
Metal anodes
Elastic constants
Density functional theory

ABSTRACT

Accurate description of the mechanical behavior of crystalline Na alloys is essential in establishing their electrochemical performance as well as their viability as anodes in Na-ion batteries. Using first principles simulations, we have investigated the intrinsic elastic properties of crystalline Na–M (M = Sn, Pb, Si and Ge) phases observed during Na intercalation. We have obtained the complete set of concentration-dependent anisotropic elastic constants as well as the average macroscopic elastic moduli of polycrystalline structures. We find that sodiation of pure M phases leads to a remarkable elastic softening that results in up to 75% deterioration of the elastic moduli. Our analysis of the electronic charge distribution demonstrates that the elastic softening during sodiation originates from a transition to weaker ionic interatomic bonding. Our results highlight the significance of the concentration dependence of the elastic moduli for the analysis of deformation behavior of Na alloy anodes of Na-ion batteries during sodiation and desodiation.

© 2012 Elsevier B.V. All rights reserved.

1. Introduction

Over the last decade, Li-ion batteries have become a mainstay for energy storage technologies [1]. The outstanding energy capacity, high volumetric density and the long cycle life of Li-ion batteries has made them the preferred choice for applications in portable electronics, and increasingly in electric vehicles [1–3]. However, forecasts of an ever increasing demand for batteries have raised questions as to whether the Li natural reserves will continue to meet industrial needs in a commercially viable manner [4]. These concerns have fueled an active search for alternatives to the Li-ion battery technologies. Among the alternatives that are being explored for this purpose, the Na-ion battery is a prime candidate. While the energy density of a Na-ion battery is generally lower than a Li-ion battery, Na has a large negative redox potential and its natural resources are abundant [4,5]. Hence, Na-ion batteries provide an attractive low-cost alternative to Li-ion batteries, especially in applications where high energy density is not the most critical design constraint [6].

Since Na is electrochemically similar to Li, efforts to identify suitable electrode materials for Na-ion batteries have largely focused on materials structurally similar to those used for electrodes in Li-ion batteries [7]. A large number of layered materials have been suggested as candidates for positive electrodes [8,9]. On the other hand, possible materials for negative electrodes (anodes) are mostly limited to carbonaceous materials, which suffer from low gravimetric capacity and poor cycle life [10,11]. Only recently, experiments have shown that Na ions can be incorporated electrochemically in metallic Sn and Pb [12,13]. The gravimetric capacity of Na-intercalated compounds $Na_{15}Sn_4$ and $Na_{15}Pb_4$ has been measured to be 845 mAh g^{-1} and 485 mAh g^{-1}, respectively [12,13], while theoretical calculations have suggested a large capacity in excess of 825 mAh g^{-1} for NaSi and NaGe compounds

* Corresponding author. Tel.: +61 3 9905 1421; fax: +61 3 9905 4940.
** Corresponding author. Tel.: +1 215 898 1558; fax: +1 215 898 2551.
E-mail addresses: vshenoy@seas.upenn.edu (V.B. Shenoy), nikhil.medhekar@monash.edu (N.V. Medhekar).

0378-7753/$ – see front matter © 2012 Elsevier B.V. All rights reserved.
http://dx.doi.org/10.1016/j.jpowsour.2012.10.044

[12,14]. Since these capacities are comparable to the state-of-the-art Li-carbon anodes, Na–M (M = Sn, Pb, Si and Ge) alloys are emerging as potential anode candidates for Na-ion batteries. As in the case of Li-ion alloy anodes [15–17], sodiation/desodiation processes in these alloys are accompanied by a drastic change in their crystal symmetries as well as volume expansion/contraction. These repetitive structural changes are known to be responsible for the loss of capacity and a low cycle life of Li–Si and Li–Sn alloys [18,19], and therefore are also expected to be a detrimental factor in the electrochemical performance of Na–M alloy anodes. It is thus crucial that the mechanical response of the Na–M alloys to sodiation/desodiation be accurately characterized.

The mechanical response of a polycrystalline material to stress fields arising from the repetitive structural changes intimately depends on the material's intrinsic elastic properties. For example, the bulk modulus (B) of a material is related to its cohesive energy and indicates resistance to bond breaking, while the shear modulus (G) can be considered as a measure of the resistance to plastic deformation [20,21]. Materials with small values for the B/G ratio are generally susceptible to brittle failures [21]. Consequently, mathematical models [22,23] used to analyze the mechanical behavior of electrode materials require knowledge of the intrinsic elastic properties of each of the Na–M alloys. In addition, recent experiments suggest that the electrode potential is strongly influenced by the stress fields associated with structural changes [24,25]. Hence, characterization of elastic properties is also important to ascertain the in-situ electrochemical performance. Thus far, no experimental or theoretical study has been performed in order to characterize the fundamental elastic properties of the Na–M alloy anode materials for Na-ion batteries.

In this article, we report on the intrinsic elastic properties of the Na–M (M = Sn, Pb, Si and Ge) alloy phases using first principles calculations. For these alloys, we consider all the crystalline phases that are typically observed in the normal battery operating temperature. During sodiation of Sn, intermetallic phases $NaSn_5$, Na_7Sn_{12}, NaSn, Na_9Sn_4 and $Na_{15}Sn_4$ form with increasing Na concentration [26], while for the Na–Pb system, $NaPb_3$, NaPb and $Na_{15}Pb_4$ phases have been observed [27]. On the other hand, we consider NaSi and NaGe, which are the only thermodynamically stable phases of Na with Si and Ge, respectively [27,28]. Here we have obtained the complete set of anisotropic elastic constants for single crystal phases as well as the orientation-averaged elastic moduli for polycrystalline phases. Our results suggest that the elastic moduli of the Na–M phases, in general, decrease linearly with the Na concentration. Moreover, we find that a large degree of sodiation leads to a remarkable elastic softening in these phases in a manner qualitatively similar to *in situ* and *ex situ* experimental observations in Li–Sn and Li–Si phases [24,29].

2. Methodology

All our calculations were performed within the framework of spin-polarized density functional theory (DFT) as implemented in the Vienna Ab Initio Simulation Package [30]. Electron exchange and correlation were described using the generalized-gradient approximation of the Perdew–Burke–Ernzerhof form [31]. Projector-augmented wave potentials were used to treat core and valence electrons [32]. The $2p^6 3s^1$, $5s^2 4d^{10} 5p^2$, $5d^{10} 6s^2 6p^2$, $3s^2 3p^2$ and $4s^2 3d^{10} 4p^2$ states were treated as valence electrons for Na, Sn, Pb, Si and Ge, respectively. In all cases, we employed a plane-wave kinetic energy cutoff of 550 eV. The Monkhorst–Pack automated mesh method was used for sampling the Brillouin zone. Convergence tests with respect to kinetic energy cutoff and Brillouin zone sampling points were carried out to ensure the total energy convergence within 1 meV atom^{-1}. The number of sampling points for the Brillouin zone of each of the Na–M phases are given in Table A.1 in the Electronic Supplementary data.

For each of the Na–M (M = Sn, Pb, Si and Ge) crystalline phases, the crystal structure information was first obtained using the crystal structure database [27,33,34]. The crystals were optimized by allowing the lattice cell vectors and the ionic positions to relax until the Hellmann–Feynman forces were less than 0.01 eV Å^{-1}. The optimized structural parameters are given in Table 1. For each alloy phase, we also computed the formation energy E_f and electrode potential Φ with respect to Na/Na$^+$ as $E_f = E(Na_xM) - [xE(Na) + E(M)]$ and $\Phi = -E_f/x$. Here, x is the number of Na atoms per M atoms, $E(Na_xM)$ is the total energy of Na_xM phase per M atoms, $E(Na)$ is the total energy of a single Na atom in bcc crystal lattice, and $E(M)$ is the total energy of a single M atom in its elemental crystal lattice. The optimized lattice parameters, as well as electrode potentials obtained from our DFT calculations, are in close agreement with the earlier experimental [35,36] and theoretical studies [37,38].

When an infinitesimally small and homogeneous deformation is applied to a crystal, its internal strain energy U can be written in terms of the strain field η_{ij} as

$$U(\eta) = U(0) + \frac{V_0}{2}\sum_{ijkl} c_{ijkl}\eta_{ij}\eta_{kl} + O\left(\eta_{ij}^3\right), \quad (1)$$

where $U(0)$ and V_0 is the internal energy and the volume of the strain-free crystal, respectively [39]. The second order elastic constants c_{ijkl} can be readily obtained from the second derivative of the internal energy as $c_{ijkl} = V_0^{-1}\partial^2 U/\partial\eta_{ij}\partial\eta_{kl}$. By employing Voigt notation for the second order strain tensor [40], Eq. (1) can be simplified as

$$U(\eta) = U(0) + \frac{V_0}{2}\sum_{ij} C_{ij}\eta_i\eta_j + O\left(\eta_i^3\right), \quad (2)$$

where C_{ij} are the second order elastic constants in Voigt notation. It can be noted that in an infinitesimally small strain limit, the internal energy of the crystal can be expressed as a second order polynomial function of the strain. Therefore, the elastic constants

Table 1
Equilibrium lattice parameters (a, b, and c, in Å), formation energy E_f (eV) and electrode potential Φ (V) for Na_xM alloys as obtained from DFT calculations.

Phase	x	Space group	a	b	c	E_f	Φ
Na–Sn							
β-Sn	0.00	$I4_1/amd$	5.95	5.95	3.21		
$NaSn_5$	0.20	$P\text{-}42_1m$	6.41	6.41	8.94	−0.127	0.63
Na_7Sn_{12}	0.58	P12/c1	13.65	9.74	17.88	−0.388	0.55
NaSn	1.00	$I4_1/acd$	10.47	10.47	17.60	−0.488	0.48
Na_9Sn_4	2.25	Cmcm	5.43	9.41	29.39	−0.665	0.29
$Na_{15}Sn_4$	3.75	$I\bar{4}3d$	13.16	13.16	13.16	−0.816	0.21
Na	∞	Im3m	4.21	4.21	4.21		
Na–Pb							
Pb	0.00	Fm3m	5.04	5.04	5.04		
$NaPb_3$	0.33	Pm3m	4.94	4.94	4.94	−0.152	0.45
NaPb	1.00	$I4_1/acd$	10.66	10.66	18.07	−0.363	0.36
$Na_{15}Pb_4$	3.75	$I\bar{4}3d$	13.34	13.34	13.34	−0.685	0.18
Na	∞	Im3m	4.21	4.21	4.21		
Na–Si							
Si	0.00	Fd3m	5.46	5.46	5.46		
NaSi	1.00	C2/c	6.58	6.06	9.70	−0.034	0.03
Na	∞	Im3m	4.21	4.21	4.21		
Na–Ge							
Ge	0.00	Fd3m	5.76	5.76	5.76		
NaGe	1.00	$P2_1/c$	6.71	11.50	10.70	−0.322	0.32
Na	∞	Im3m	4.21	4.21	4.21		

can be readily obtained from the second order coefficient of a polynomial fit to the internal energy with respect to the strain component.

In order to calculate the elastic constants of Na–M crystals, we applied a specific set of homogeneous and infinitesimal strains depending on the crystalline symmetry in each case. For example, three independent elastic constants for cubic crystals were obtained using uniaxial distortion, isotropic volumetric distortion and pure shear. In a similar manner, a specific set of deformation modes was selected to determine six, nine, and thirteen independent elastic constants for tetragonal, orthorhombic, and monoclinic crystals, respectively. The deformation modes used for each crystal symmetry as well as the relationship between the elastic constants and the second order coefficients of the polynomial fits are outlined in Table A.2 in the Electronic Supplementary data. The total energy of the strained crystal was obtained from DFT calculations by allowing atomic positions to relax. The elastic constants were then obtained from the polynomial fit to the internal energy.

3. Results and discussion

The second order elastic constants of Na–M (M = Sn, Pb, Si and Ge) crystalline phases obtained from our DFT calculations are presented in Table 2. The calculated elastic constants for pure Na, Sn, Pb, Si and Ge phases are in agreement with both experimental measurements (see Table 3) and theoretical calculations [41,42]. It should be noted that the values presented in Table 2 correspond to the elastic constants of *single crystal* structures. However, the realistic microstructure of negative electrode alloys as observed in experiments is *polycrystalline* with numerous single crystal grains oriented randomly with respect to each other [29]. It is therefore important to relate the single crystal elastic constants obtained from our DFT calculations (Table 2) to the aggregate elastic constants of polycrystalline materials. To achieve this, continuum theories developed by Voigt and Reuss [43] provide a convenient way of obtaining the aggregate elastic constants. By following the Voigt's or Reuss' method, the effective isotropic elastic constants are obtained by averaging the single crystal elastic constants over all possible orientations, with the assumption that all grains are under uniform strain or stress, respectively. Hill [43] showed that the Voigt and Reuss methods give upper and lower bounds on the elastic properties of macroscopically isotropic crystals, respectively, and suggested using their arithmetic means to obtain realistic estimates of elastic properties of polycrystalline microstructure. Here, the Young's modulus (E), shear modulus (G), and bulk modulus (B) of polycrystalline Na–M phases using the Voigt, Reuss and Hill methods have been computed as shown in Table 4. As seen from Table 3, our calculated values for polycrystalline elastic moduli of pure phases are in good agreement with experiments. The orientation averaged Poisson's ratios are provided in Table A.3 in the Electronic Supplementary data.

Table 3
Experimental values of single crystal elastic constants (C_{ij}) as well as polycrystalline moduli for pure Sn, Pb, Si, Ge and Na phases. The values for Sn are obtained from [49,50] while the rest are reported by Simmons [51]. All values are in GPa.

Phase	C_{11}	C_{33}	C_{44}	C_{66}	C_{12}	C_{13}	B_H	E_H	G_H
β-Sn	73.50	87.60	22.00	22.65	23.40	28.00	45.00	51.01	17.93
Pb	55.54		19.42		45.42		38.50	33.70	12.20
Si	167.72		80.36		64.98		99.20	164.80	67.30
Ge	131.50		68.40		49.48		76.80	135.00	55.90
Na	8.21		5.77		6.83		7.30	7.90	3.00

It is clear from Table 4 that even a small degree of sodiation in pure phases leads to a significant drop in the elastic moduli. In order to systematically understand the degree of elastic softening in Na–M alloys upon sodiation, we have plotted Young's and shear moduli as a function of the Na fraction $y = x/(x+1)$ in Fig. 1. Here, $y = 0$ and $y = 1$ represents the pure polycrystalline M phase and Na phase, respectively. It can be seen that the elastic moduli strongly depend on the Na fraction for all Na–M phases. In general, the moduli show an approximately linear dependence on the Na fraction, which suggests that approximate elastic moduli of the alloy phases can be obtained using a linear combination of the moduli of constituent elements. As we explain next, however, the Young's and shear moduli of Na–Sn and Na–Pb phases do not decrease with the Na fraction in a strictly monotonic manner.

Upon sodiation of pure Sn, the elastic moduli reduce sharply till the formation of the second intermetallic phase Na_7Sn_{12} ($y \sim 0.36$). On further sodiation, both the Young's modulus and shear moduli vary in a narrow range of 15–25 GPa and 5–10 GPa, respectively. For $Na_{15}Sn_4$, the phase with the largest sodium concentration, the

Table 2
Elastic constants C_{ij} (in GPa) for single crystal Na_xM phases.

Phase	C_{11}	C_{22}	C_{33}	C_{44}	C_{55}	C_{66}	C_{12}	C_{13}	C_{23}	C_{15}	C_{25}	C_{35}	C_{46}
Na–Sn													
β-Sn	72.22	72.22	87.77	19.66	19.66	23.71	33.55	30.59	30.59				
$NaSn_5$	55.06	55.06	42.68	18.28	18.28	17.15	30.68	13.99	13.99				
Na_7Sn_{12}	52.01	40.2	26.67	11.54	5.94	11.33	17.84	11.21	24.13	0.50	2.53	2.55	3.01
NaSn	28.29	28.29	26.94	11.63	11.63	13.22	12.13	11.93	11.93				
Na_9Sn_4	39.71	39.47	43.48	8.82	7.74	4.04	14.56	4.07	5.27				
$Na_{15}Sn_4$	18.85	18.85	18.85	5.78	5.78	5.78	6.86	6.86	6.86				
Na	8.46	8.46	8.46	5.78	5.78	5.78	6.86	6.86	6.86				
Na–Pb													
Pb	52.74	52.74	52.74	17.68	17.68	17.68	36.14	36.14	36.14				
$NaPb_3$	37.60	37.60	37.60	15.00	15.00	15.00	30.61	30.61	30.61				
NaPb	25.93	25.93	27.68	11.47	11.47	10.27	8.54	9.73	9.73				
$Na_{15}Pb_4$	20.46	20.46	20.46	7.62	7.62	7.62	9.48	9.48	9.48				
Na	8.46	8.46	8.46	5.78	5.78	5.78	6.86	6.86	6.86				
Na–Si													
Si	153.22	153.22	153.22	74.70	74.70	74.70	58.87	58.87	58.87				
NaSi	38.8	41.96	45.48	13.33	14.70	18.08	8.19	16.01	15.29	−1.86	0.55	0.11	−0.20
Na	8.46	8.46	8.46	5.78	5.78	5.78	6.86	6.86	6.86				
Na–Ge													
Ge	104.82	104.82	104.82	56.62	56.62	56.62	36.50	36.50	36.50				
NaGe	32.00	25.34	6.88	40.44	36.05	14.77	9.75	6.38	6.88	−0.35	3.83	−9.64	1 6.73
Na	8.46	8.46	8.46	5.78	5.78	5.78	6.86	6.86	6.86				

Table 4
Bulk modulus (B), Young's modulus (E), and shear modulus (G) of polycrystalline Na_xM alloys obtained using Reuss (R), Voigt (V), and Hill (H) averaging methods. A^U denotes the universal anisotropy factor. All moduli are in GPa.

Phase	B_V	B_R	E_V	E_R	G_V	G_R	B_H	E_H	G_H	B_H/G_H	A^U
Na–Sn											
β-Sn	46.85	46.63	56.56	55.7	21.77	21.41	46.74	56.13	21.59	2.17	0.08
$NaSn_5$	28.38	17.02	42.95	41.26	17.02	16.40	29.20	42.10	16.71	1.74	0.22
Na_7Sn_{12}	25.03	21.43	26.81	20.22	10.14	7.53	23.23	23.51	8.83	2.62	1.90
NaSn	17.28	17.26	26.13	25.14	10.46	9.99	17.27	25.63	10.23	1.85	0.23
Na_9Sn_4	18.94	18.87	27.02	21.19	10.70	8.07	18.91	24.11	9.38	2.01	1.63
$Na_{15}Sn_4$	13.83	13.83	15.75	14.26	6.01	5.37	13.83	15.01	5.69	2.42	0.59
Na	7.39	7.39	8.46	9.70	4.62	3.78	7.39	7.16	2.72	2.71	6.43
Na–Pb											
Pb	41.67	41.67	37.61	33.29	13.93	12.17	41.68	35.45	13.06	3.19	0.72
$NaPb_3$	32.94	32.94	28.23	18.23	10.40	6.47	32.94	23.23	8.43	3.90	3.02
NaPb	15.06	15.02	24.72	24.36	10.08	9.90	15.04	24.54	9.99	1.50	0.09
$Na_{15}Pb_4$	13.14	13.14	17.33	16.95	6.77	6.59	13.14	17.14	6.68	1.96	0.13
Na	7.39	7.39	8.46	9.70	4.62	3.78	7.39	7.16	2.72	2.71	6.43
Na–Si											
Si	90.32	90.32	154.70	148.5	63.68	60.56	90.32	151.60	62.12	1.45	0.25
NaSi	22.80	23.18	36.92	36.27	15.00	14.63	22.99	36.59	14.82	1.55	0.11
Na	7.39	7.39	8.46	9.70	4.62	3.78	7.39	7.16	2.72	2.71	6.43
Na–Ge											
Ge	60.62	60.62	112.49	106.53	47.23	44.12	60.62	109.51	45.68	1.32	0.35
NaGe	16.29	16.00	47.50	30.84	23.42	13.08	16.15	39.17	18.25	0.88	3.19
Na	7.39	7.39	8.46	9.70	4.62	3.78	7.39	7.16	2.72	2.71	6.43

Young's and shear moduli are reduced by 74% and 70% compared to pure Sn, respectively. A similar behavior can be observed for Na–Pb system—the Young's and shear moduli of all Na_xPb alloys vary in the same narrow range. The deviation of the elastic moduli of Na_7Sn_{12}, Na_9Sn_4 and $NaPb_3$ phases from linear trendlines in Fig. 1 can be attributed to their anisotropic single crystal elastic constants. To quantify the relative anisotropies of all Na–M phases, we have computed the universal anisotropy factor A^U (see Table 4), which measures the extent of elastic anisotropy in each phase [44]. Among the intermetallic Na–Sn and Na–Pb phases, Na_7Sn_{12}, Na_9Sn_4 and $NaPb_3$ exhibit relatively large elastic anisotropy (large values of A^U), which is consistent with the deviation of their moduli from the linear trend shown in Fig. 1.

The elastic softening in Na–Sn and Na–Pb phases upon sodiation as seen in Fig. 1 is qualitatively similar to the elastic softening in Li–Sn phases [45]. There is one remarkable difference: the Young's and shear moduli of Li_xSn phases show an abrupt increase for $x \sim 2.33$ (where the moduli are even greater than the moduli of Sn), followed by a drastic softening upon further lithiation. As seen from Fig. 1, however, the elastic softening in Na–Sn and Na–Pb phases is gradual. Since the internal stresses that are generated during the phase transformation during intercalation/deintercalation depend on the elastic moduli, Na–Sn and Na–Pb phases are likely to be more amenable to gradual structural transformations compared to Li–Sn phases due to the absence of any built-up internal stresses associated with sharp changes in elastic moduli.

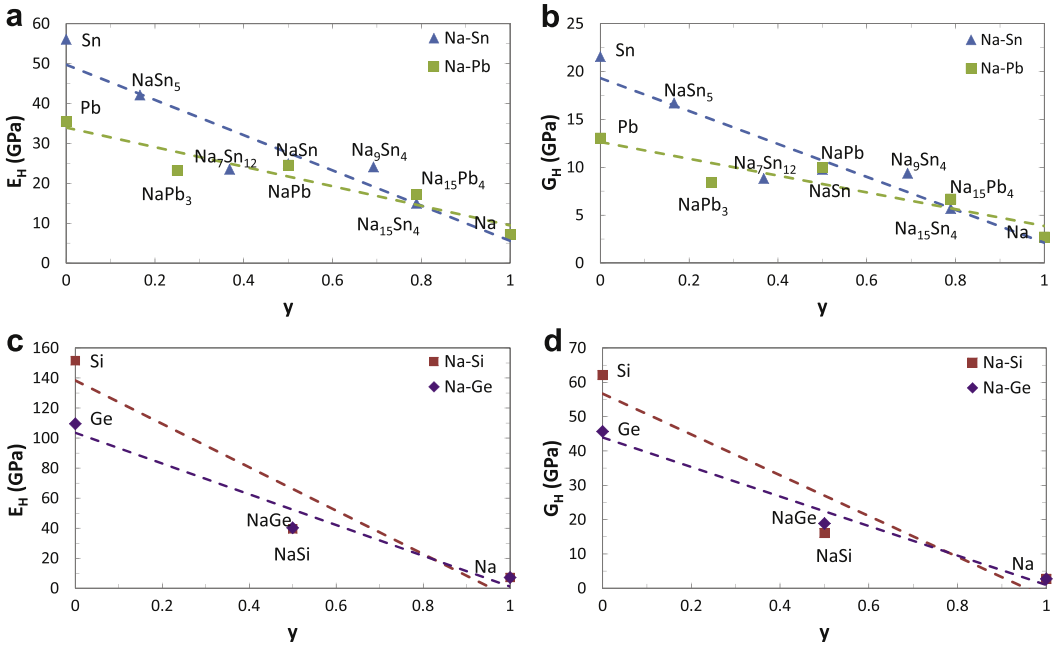

Fig. 1. Young's modulus (E_H) and shear modulus (G_H) of Na_xM alloys vs. Na fraction y, (a, b) M = (Sn, Pb) and (c, d) M = (Si, Ge).

Compared to Na–Sn and Na–Pb phases, the elastic softening in Na–Si and Na–Ge is more severe as seen from Fig. 1(c,d). Upon sodiation, the elastic moduli of Si and Ge are immediately reduced by approximately 73% and 60%, respectively. Furthermore, as seen from Table 2, both the NaSi and NaGe alloys are characterized by a low value of B_H/G_H compared to Na–Sn and Na–Pb alloys. Since low values for this ratio indicate a low resistance toward brittle failures, our results suggest that the Na–Si and Na–Ge systems are susceptible to fracture and disconnection between particles upon sodiation. The degradation of electrode structure as a result of brittle fracture and the subsequent capacity loss has been reported in Li–Si alloys [29].

In order to understand the atomic-level origins of the elastic softening in Na–M phases upon increasing sodium concentration, we next analyze their electronic structures obtained from our DFT calculations. The electronic charge distribution in Na–M (M = Sn, Pb, Si, Ge) phases are shown through Figs. 2–4. From the electronic charge distribution, the net charges on each atom were then obtained using Bader charge population analysis [46]. As seen from Table 5, each Na atom donates a large fraction (0.67–0.81 e^-) of its electrons to neighboring M atoms. It can be noted that the net charge on Na is smaller than the net charge on Li in crystalline Li-ion anodes (typically greater than 0.8 e^-) [45,47,48], which can be attributed to the larger diameter of the Na ion. On the other hand, M atoms adopt a charge state that intimately depends on their bonding interactions with neighboring Na and M atoms. For instance, in the case of $NaSn_5$, each Sn atom adopts one of the three distinct charge states depending on the number of bonds it forms with neighboring Sn atoms. For Na_7Sn_{12} and Na_9Sn_4 phases, Sn atoms acquire a range of net charges depending on the near-neighbor bond lengths. For NaSn, $Na_{15}Sn_4$, NaSi and all Na–Pb phases, all M atoms adopt essentially identical charge states.

While the electronic charge distributions for each of the Na–M systems as shown in Figs. 2–4 are unique, they are characterized by the following general observations: (1) M atoms nearest to a Na atom typically have the largest net charge, indicating that the interaction between Na and M has a strong ionic character, and (2) with increasing Na concentration, a greater number of M atoms have a large net charge as a result of being surrounded by the increasingly larger number of Na atoms. These observations together essentially suggest that upon sodiation, M–M bonds are being replaced with ionic Na–M bonds.

The gradual transition to ionic bonding with increasing Na concentration can be further understood from the evolution of the charge density isosurfaces shown in Figs. 2–4. Taking the Na–Sn system as an illustrative example, we next elucidate the correlation between the elastic softening and the interatomic bonding. As seen from Fig. 2, while both β-Sn and Na are metallic, their electronic charge distribution is markedly different. The electronic orbitals of each Sn atom overlap with those of the six neighboring Sn atoms resulting in significant sharing of the electronic charge. Thus, the Sn–Sn bond has a weakly covalent and directional

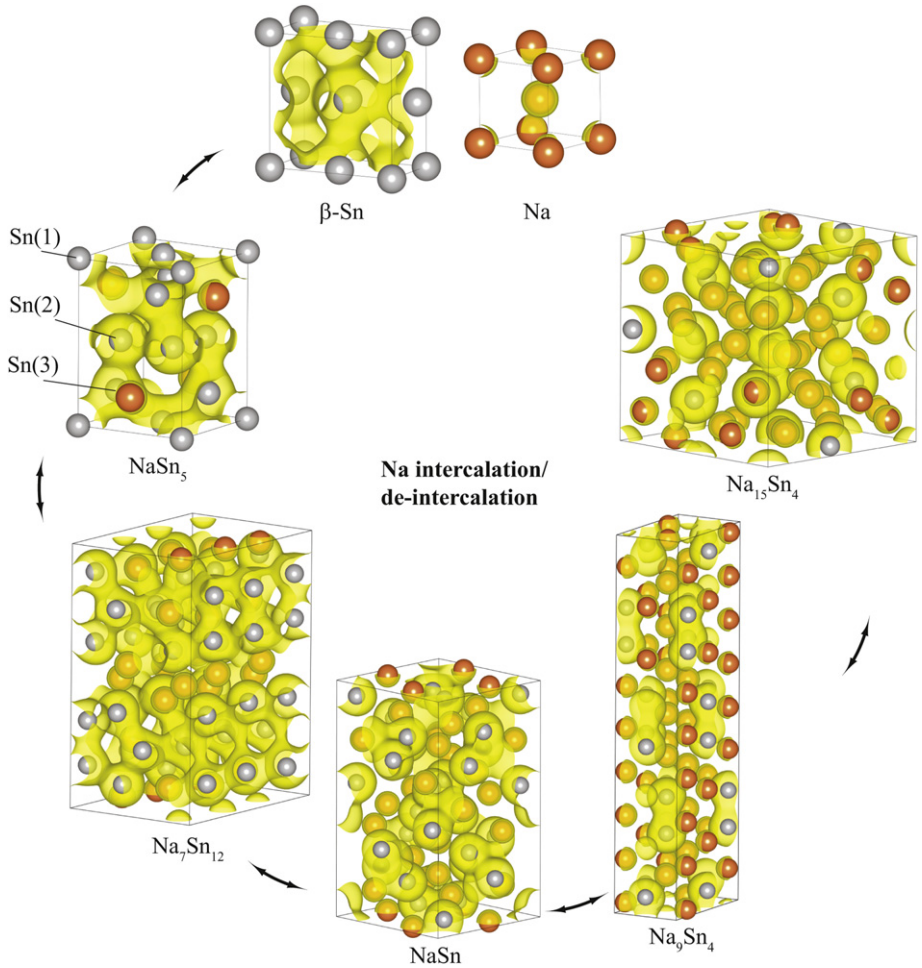

Fig. 2. Electronic charge density distribution in Na_xSn alloys. Yellow isosurfaces are plotted at a density of 0.02 e^-/bohr^3. Orange and silver spheres denote Na and Sn atoms, respectively. (For interpretation of the references to colour in this figure legend, the reader is referred to the web version of this article.)

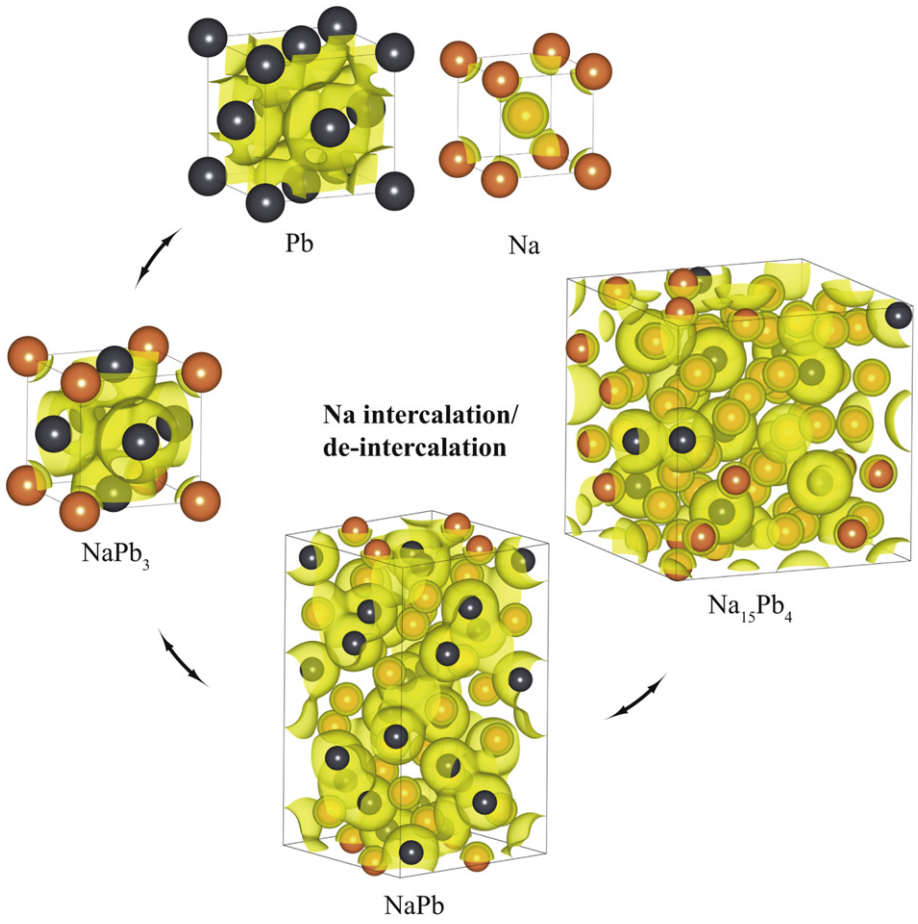

Fig. 3. Electronic charge density distribution in Na_xPb alloys. Yellow isosurfaces are plotted at a density of 0.015 e^-/bohr^3. Orange and gray spheres denote Na and Pb atoms, respectively. (For interpretation of the references to colour in this figure legend, the reader is referred to the web version of this article.)

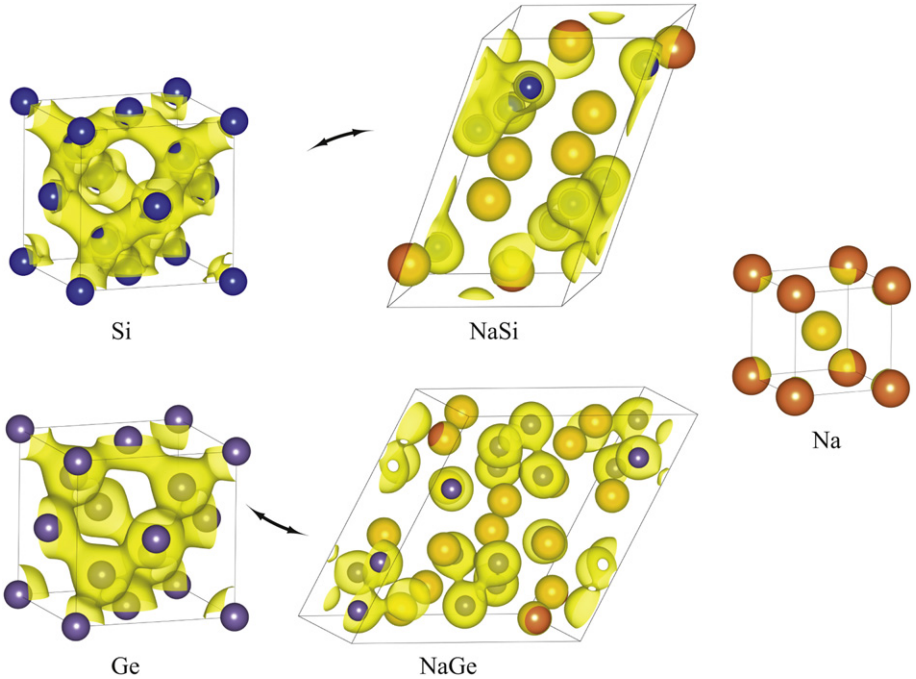

Fig. 4. Electronic charge density distribution in Na_xSi and Na_xGe alloys. Yellow isosurfaces are plotted at a density of 0.05 e^-/bohr^3. Orange, blue and purple spheres denote Na, Si and Ge atoms, respectively. (For interpretation of the references to colour in this figure legend, the reader is referred to the web version of this article.)

Table 5
Net charges (e^-) on Na and M atoms in Na_xM alloy phases obtained using Bader charge population analysis.

Phase	Net charge on	
	Na atoms	M atoms
$NaSn_5$	0.80	Sn(1): −0.11, Sn(2): −0.16, Sn(3): −0.22
Na_7Sn_{12}	0.75–0.81	Sn: −0.10 to −1.1
NaSn	0.78	Sn: −0.78
Na_9Sn_4	0.73	Sn: −1.50 to −1.7
$Na_{15}Sn_4$	0.70	Sn: −2.50
$NaPb_3$	0.78	Pb: −0.26
NaPb	0.76	Pb: −0.76
$Na_{15}Pb_4$	0.67	Pb: −2.50
NaSi	0.80	Si: −0.80
NaGe	0.79	Ge: −0.68 to −0.88

character. In contrast, Na displays a minimal sharing of electrons—almost the entire electronic charge is distributed over a small localized region around Na ions. Furthermore, the Sn–Sn bond length is smaller compared to the Na–Na bond (3.02 Å vs. 3.64 Å), while Sn atoms have four valence electrons in contrast to the single valence electron for Na. Thus, due to the sharing of larger number of electrons, the Sn–Sn bonds are expected to be stiffer than the Na–Na bonds, which is reflected in the relatively large difference between their elastic moduli as shown in Table 4.

It readily follows that replacing a Sn–Sn bond with a relatively weak ionic Na–Sn bond should result in a reduction in the elastic moduli. This is evident in the case of $NaSn_5$, where every Sn atom has on an average only five Sn–Sn bonds compared to six in β-Sn. With increasing Na concentration, the average number of Sn–Sn bonds for every Sn atom further reduces to three (in Na_7Sn_{12}), two (in NaSn), and to just one (in Na_9Sn_4). Lastly, for the phase with the largest Na concentration, $Na_{15}Sn_4$, every Sn atom is completely surrounded by Na atoms, resulting in an elastic moduli comparable to that of pure Na. A similar gradual transition from covalent bonding to ionic bonding—along with the reduction in their elastic moduli—can also be seen in Na–Pb (Fig. 3), Na–Si and Na–Ge (Fig. 4) systems. Thus, the observed elastic softening in Na–M phases upon sodiation is a direct consequence of the increasing relative population of weaker Na–M bonds. A similar transition to ionic bonding in high lithium concentrations has been reported in Li–Sn [45] and Li–Si [47] alloys.

Our analysis of the electronic charge distribution can also explain almost identical elastic behavior of some of the Na-metal phases. For example, it is evident from Table 4 that the elastic moduli of the NaSn and $Na_{15}Sn_4$ phases are nearly equal to the moduli of their Na–Pb counterparts, viz., NaPb and $Na_{15}Pb_4$. It is clear that these phases have similar crystal structures (Table 1), while the net charges on Na and M atoms are also identical (Table 5). Since both Sn and Pb have four valence electrons, the sharing of electrons between neighboring atoms is also very similar (Figs. 2 and 3), thus leading to almost identical elastic moduli. These observations again highlight the central role played by the electronic charge distribution in governing the macroscopic elastic behavior.

4. Conclusions

In conclusion, we have obtained the most fundamental elastic properties of Na–M (M = Sn, Pb, Si, Ge) alloys for anodes in Na-ion batteries. Our results show that while their elastic moduli in general decrease linearly with increasing Na concentration, the elastically anisotropic phases show a deviation from this trend. A large concentration of Na leads to a drastic elastic softening of the alloy phases—the elastic moduli of Na-rich phases of Sn, Pb, Si and Ge are reduced by 60–75% compared to the pure phases. Based on the analysis of electronic charge distribution, we have shown that the elastic softening in all Na–M phases can be attributed to the evolution of the nature of interatomic bonding with increasing Na concentration. While the deterioration of the elastic moduli upon sodiation may be a limiting factor for the structural stability of anode materials, the elastic constants as well as their functional relationship with Na concentration presented here can be readily employed in simple continuum models for deformation and fracture of Na-ion battery electrode materials. The quantitative framework provided by these models can systematically inform the design of Na-ion electrode architectures as well as the choice of binders for improving the mechanical stability of the electrode materials.

Acknowledgment

MM, JD and NM gratefully acknowledge computational support from Monash University Sun Grid, Multi-modal Australian Sciences Imaging and Visualisation Environment and the Australian National Computing Infrastructure. VS gratefully acknowledges support from the NSF and DOE.

Appendix A. Supplementary data

Supplementary data related to this article can be found at http://dx.doi.org/10.1016/j.jpowsour.2012.10.044.

References

[1] V. Etacheri, R. Marom, R. Elazari, G. Salitra, D. Aurbach, Energy Environ. Sci. 4 (2011) 3243–3262.
[2] D. Larcher, S. Beattie, M. Morcrette, K. Edstroem, J. Jumas, J. Tarascon, J. Mater. Chem. 17 (2007) 3759–3772.
[3] G. Jeong, Y. Kim, H. Kim, Y. Kim, H. Sohn, Energy Environ. Sci. 4 (2011) 1986–2002.
[4] V. Palomares, P. Serras, I. Villaluenga, K. Hueso, J. Carretero-González, T. Rojo, Energy Environ. Sci. 5 (2012) 5884–5901.
[5] S. Ong, V. Chevrier, G. Hautier, A. Jain, C. Moore, S. Kim, X. Ma, G. Ceder, Energy Environ. Sci. 4 (2011) 3680–3688.
[6] J. Liu, J. Zhang, Z. Yang, J. Lemmon, C. Imhoff, G. Graff, L. Li, J. Hu, C. Wang, J. Xiao, et al., Adv. Funct. Mater, in press.
[7] S. Kim, D. Seo, X. Ma, G. Ceder, K. Kang, Adv. Energy Mater. 2 (2012) 710–721.
[8] M. Slater, D. Kim, E. Lee, C. Johnson, Adv. Funct. Mater, in press.
[9] B. Ellis, L. Nazar, Curr. Opin. Solid State Mater. Sci. 16 (2012) 168–177.
[10] S. Wenzel, T. Hara, J. Janek, P. Adelhelm, Energy Environ. Sci. 4 (2011) 3342–3345.
[11] K. Tang, L. Fu, R. White, L. Yu, M. Titirici, M. Antonietti, J. Maier, Adv. Energy Mater. 2 (2012) 873–877.
[12] T. Tran, M. Obrovac, J. Electrochem. Soc. 158 (2011) A1411–A1416.
[13] S. Komaba, Y. Matsuura, T. Ishikawa, N. Yabuuchi, W. Murata, S. Kuze, Electrochem. Commun. 21 (2012) 65–68.
[14] V. Chevrier, G. Ceder, J. Electrochem. Soc. 158 (2011) A1011–A1014.
[15] J. Yang, M. Winter, J. Besenhard, Solid State Ionics 90 (1996) 281–287.
[16] J. Besenhard, J. Yang, M. Winter, J. Power Sources 68 (1997) 87–90.
[17] W. Zhang, J. Power Sources 196 (2011) 13–24.
[18] U. Kasavajjula, C. Wang, A. Appleby, J. Power Sources 163 (2007) 1003–1039.
[19] M. Winter, J. Besenhard, Electrochim. Acta 45 (1999) 31–50.
[20] D. Clerc, J. Phys. Chem. Solids 60 (1999) 83–102.
[21] S. Pugh, Philos. Mag. 45 (1954) 823–843.
[22] Y. Cheng, M. Verbrugge, J. Power Sources 190 (2009) 453–460.
[23] J. Christensen, J. Newman, J. Solid State Electrochem. 10 (2006) 293–319.
[24] J. Chen, S. Bull, S. Roy, H. Mukaibo, H. Nara, T. Momma, T. Osaka, Y. Shacham-Diamand, J. Phys. D Appl. Phys. 41 (2008) 025302.
[25] H. Mukaibo, T. Momma, Y. Shacham-Diamand, T. Osaka, M. Kodaira, Electrochem. Solid State Lett. 10 (2007) A70.
[26] J. Sangster, C. Bale, J. Phase Equilib. Diffus. 19 (1998) 76–81.
[27] M. Tegze, J. Hafner, Phys. Rev. B 39 (1989) 8263–8274.
[28] J. Sangster, A. Pelton, J. Phase Equilib. 18 (1997) 295–297.
[29] V. Sethuraman, M. Chon, M. Shimshak, V. Srinivasan, P. Guduru, J. Power Sources 195 (2010) 5062–5066.
[30] G. Kresse, J. Furthmüller, Phys. Rev. B 54 (1996) 11169–11186.
[31] J. Perdew, K. Burke, M. Ernzerhof, Phys. Rev. Lett. 77 (1996) 3865–3868.
[32] P. Blöchl, Phys. Rev. B 50 (1994) 17953–17979.
[33] W. Pearson, vols. I and II, Pergamon Press, Oxford, 1964, 1967, 1958.
[34] M. Tegze, J. Hafner, Phys. Rev. B 40 (1989) 9841.

[35] W. Pearson, A Handbook of Lattice Spacings and Structures of Metals and Alloys, vol. 4, 1964.
[36] T. Jow, L. Shacklette, M. Maxfield, D. Vernick, J. Electrochem. Soc. 134 (1987) 1730–1733.
[37] M. Dacorogna, M. Cohen, Phys. Rev. B 34 (1986) 4996.
[38] S. Shang, A. Saengdeejing, Z. Mei, D. Kim, H. Zhang, S. Ganeshan, Y. Wang, Z. Liu, Comput. Mater. Sci. 48 (2010) 813–826.
[39] D. Wallace, Thermodynamics of Crystals, Dover Pubns, 1998.
[40] L. Landau, E. Lifshitz, Theory of Elasticity, third ed., Butterworth-Heinemann, Oxford, UK, 1986.
[41] T. Suzuki, A. Granato, J. Thomas Jr., Phys. Rev. 175 (1968) 766.
[42] M. Łopuszyński, J. Majewski, Phys. Rev. B 76 (2007) 045202.
[43] H.M. Lebetter, Handbook of Elastic Properties of Solids, Liquids and Gases, vol. 3, 2001.
[44] S. Ranganathan, M. Ostoja-Starzewski, Phys. Rev. Lett. 101 (2008) 55504.
[45] M. Stournara, P. Guduru, V. Shenoy, J. Power Sources 208 (2012) 165–169.
[46] R. Bader, Atoms in Molecules: A Quantum Theory, Int Monogr Chem, Oxford University Press, 1990.
[47] V. Shenoy, P. Johari, Y. Qi, J. Power Sources 195 (2010) 6825–6830.
[48] C. Chou, H. Kim, G. Hwang, J. Phys. Chem. C 115 (2011) 20018–20026.
[49] W. Mason, H. Bömmel, J. Acoust. Soc. Am. 28 (1956) 930–943.
[50] F. Yang, J. Li, Lead-free Electron. Solders 18 (2007) 191–210.
[51] G. Simmons, H. Wang, Single Crystal Elastic Constants and Calculated Aggregate Properties (1971).